

Individual low-energy toroidal dipole state in ^{24}Mg

V.O. Nesterenko¹, A. Repko², J. Kvasil³, and P.-G. Reinhard⁴

¹ *Laboratory of Theoretical Physics, Joint Institute for Nuclear Research, Dubna, Moscow region, 141980, Russia*

² *Department of Nuclear Physics, Institute of Physics SAS, 84511, Bratislava, Slovakia*

³ *Institute of Particle and Nuclear Physics, Charles University, CZ-18000, Prague, Czech Republic and*

⁴ *Institut für Theoretische Physik II, Universität Erlangen, D-91058, Erlangen, Germany*

(Dated: March 13, 2022)

The low-energy dipole excitations in ^{24}Mg are investigated within the Skyrme quasiparticle random-phase-approximation (QRPA) for axial nuclei. The calculations with the force SLy6 reveal a remarkable feature: the lowest $I^\pi K = 1^-1$ excitation ($E = 7.92$ MeV) in ^{24}Mg is a vortical toroidal state (TS) representing a specific vortex-antivortex realization of well-known spherical Hill's vortex in a strongly deformed axial confinement. This is a striking example of an *individual* TS which can be much easier discriminated in experiment than the toroidal dipole resonance embracing many states. The TS acquires the lowest energy due to the huge prolate axial deformation in ^{24}Mg . The result persists for different Skyrme parameterizations (SLy6, SVbas, SkM*). We analyze spectroscopic properties of the TS and its relation with the cluster structure of ^{24}Mg . Similar TS could exist in other highly prolate light nuclei. They could serve as promising tests for various reactions to probe a vortical (toroidal) nuclear flow.

The toroidal [1, 2] dipole resonance (TDR) in nuclei was predicted about 40 years ago and since that time it is a subject of a permanent high interest, see [3–5] for early and [6–10] for recent self-consistent studies. The resonance demonstrates a variety of intriguing properties. i) Its computed nuclear current [2, 10–13] forms a torus-shaped vortex ring where the current exhibits small-amplitude vortical oscillation around a closed loop line, see Fig. 1(a,b). It reminds so-called spherical Hill's vortex well known in hydrodynamics [14, 15]. The difference is that in Hill's vortex the flow spins around the torus while in TDR the current oscillates along the same streamlines. ii) TDR is the only known example of the *intrinsic electric vortical* flow in nuclei [2, 5, 8]. The toroidal strength can be used as measure of the nuclear dipole vorticity [8]. iii) TDR is the transversal "zero sound" mode with the features of an *elastic* medium [11, 12]. iv) TDR perhaps is the source of so-called pygmy dipole resonance [7, 9]. v) TDR is coupled [16] to the irrotational compression dipole resonance (CDR) [17, 18]. Furthermore, since TDR is located near particle emission thresholds, it can affect reaction rates important for nucleosynthesis [19, 20]. Toroidal modes and moments are discussed in solid state physics [21], areas of metamaterials, plasmonics and nanophotonics (see [22] and refs. therein), neutron stars [23], physics of anapole and dark matter [24]. Altogether, toroidal modes are of relevance to various areas of physics.

Though TDR and CDR are *second-order* dipole modes (i.e. related to $r^3 Y_{1m}$ field instead of $r Y_{1m}$ [6]), they dominate in the isoscalar ($T=0$) dipole channel of nuclear excitations and are supposed to constitute the low- and high-energy parts of the isoscalar giant dipole resonance (IS-GDR) [3–5, 25] observed in (α, α') reaction [26–28]. Following our recent calculations [9, 10], the usual interpretation of the toroidal part of IS-GDR experimental data can be disputed. So, identification of the TDR is

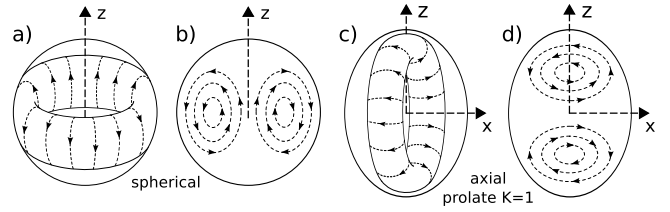


FIG. 1: Schematic toroidal dipole flow in spherical nuclei (a-b) and axial nuclei in states with $K=1$ (c-d). a) Current lines (arrows) lie on the torus surface with the axial z -axis determined by an external field. b) Toroidal flow in a plane embracing z -axis. c) Toroidal flow for $K=1$ states (for $K=0$ states the flow is like in the plot a)). d) Toroidal flow for $K=1$ states in z - x plane.

still an open problem. This substantially complicates exploration of toroidal excitations.

In this connection, we propose a new route to study the toroidal mode: to switch the experimental and theoretical effort from TDR (embracing many states and masked by other multipole modes [26–28]) to *individual* well-separated low-energy toroidal states (TS). As shown below, such TS can exist in low-energy spectra of light nuclei with a strong axial prolate deformation. What is of a crucial importance, these states can be easily discriminated and identified. Using individual TS, we could get new possibilities for testing various reactions as probes of a nuclear vortical flow. Besides we could get the answer to the important question of a general interest: how does Hill's vortex look in the limit of strongly deformed axial confinement. As shown below, the torus vortex ring (Fig. 1c-d) is converted to the vortex-antivortex pair.

This idea can be realized using specific deformation features of the isoscalar toroidal mode. As shown in [9, 10], the prolate axial deformation splits the mode into $K=0$ and $K=1$ branches and downshifts $K=1$ strength

to form a strong low-energy toroidal $K=1$ peak. The effect can be especially strong in ^{24}Mg with its extremely large axial prolate deformation $\beta=0.605\pm0.008$ [29] and a sparse spectrum below the particle thresholds. Just these two factors offer a chance to find an individual low-energy $E1(K=1)$ TS.

Our calculations are performed within the self-consistent quasiparticle random-phase-approximation (QRPA) method based on the Skyrme functional [30]. The QRPA code for axial nuclei [31] employs 2D mesh in cylindrical coordinates. The calculation box extends over three times the nuclear radius. The mesh size is 0.4 fm. The single-particle spectrum embraces all levels from the bottom of the potential well up to +55 MeV. The volume monopole pairing is treated at the BCS level [10]. We implement a representative set of Skyrme parameterizations (SLy6 [32], SVbas [33] and SkM* [34]) with various nuclear matter features. SLy6 is used as a main tool since it gives a good description of the isovector giant dipole resonance (IV-GDR) in medium-heavy [35] and light [36] nuclei, including ^{24}Mg [37].

Various models [43–47] predict a weak triaxial softness in the ground state of ^{24}Mg and more triaxiality in its positive-parity excitations. Concerning the lowest dipole states [47], the triaxiality was found essential for the $K=0$ but negligible for $K=1$. Here we mainly address the lowest dipole $K=1$ state and effects caused by very large *axial* prolate deformation. So, to simplify the problem, we base our QRPA analysis on the axial shape of ^{24}Mg . The equilibrium axial quadrupole deformation is obtained by minimization of the total nuclear energy in the ground state. This gives deformation parameters $\beta=0.536$ (SLy6), 0.525 (SVbas), and 0.493 (SkM*) in a good agreement (best for SLy6) with the value $\beta=0.605\pm0.008$ obtained from $B(E2) \uparrow$ measurements [29].

Since the toroidal and compression modes are coupled [16], we consider both of them. Their responses are treated in terms of the reduced transition probabilities $B_\nu(E1K, \alpha) = (2 - \delta_{K,0}) |\langle \nu | \hat{M}_\alpha(E1K) | 0 \rangle|^2$ where $|\nu\rangle$ is the wave function of the ν -th QRPA dipole state. The toroidal ($\alpha = \text{tor}$) and compression ($\alpha = \text{com}$) transition operators have the form [6, 7]

$$\hat{M}_{\text{tor}}(E1K) = \frac{-1}{10\sqrt{2}c} \int d^3r r [r^2 + d^s + d_K^a] \mathbf{Y}_{11K} \cdot (\nabla \times \hat{\mathbf{j}}), \quad (1)$$

$$\hat{M}_{\text{com}}(E1K) = \frac{-i}{10c} \int d^3r r [r^2 + d^s - 2d_K^a] Y_{1K} (\nabla \cdot \hat{\mathbf{j}}), \quad (2)$$

where $\hat{\mathbf{j}}(\mathbf{r})$ is operator of the isoscalar nuclear current involving convection and magnetization parts (with effective charges $e_{n,p}^{\text{eff}} = 0.5$, g-factors $g_{n,p}^s = 0.88$, and quenching $q=0.7$ [6, 25]); $\mathbf{Y}_{11K}(\hat{\mathbf{r}})$ and $Y_{1K}(\hat{\mathbf{r}})$ are vector and ordinary spherical harmonics; $d^s = -5/3 \langle r^2 \rangle_0$ is the center-of-mass corrections (c.m.c.) in spherical nuclei [6];

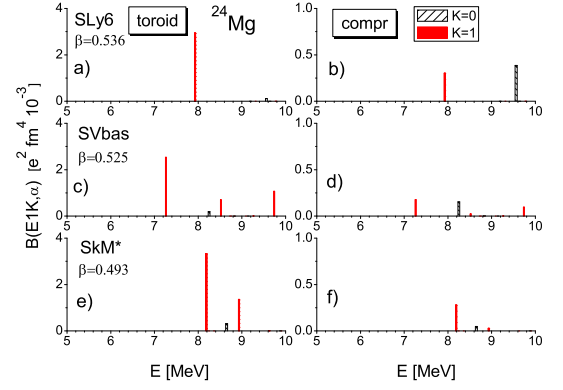


FIG. 2: Toroidal (left) and compression (right) $B(E1, \alpha)$ -values in ^{24}Mg , calculated with SLy6 (top), SVbas (middle) and SkM* (bottom) forces. Responses for $K=0$ ($K=1$) are depicted by sparse black (filled red) bars. Deformation parameters are shown for each force.

$d_K^a = \sqrt{4\pi/45} \langle r^2 Y_{20} \rangle_0 (3\delta_{K,0} - 1)$ is the additional c.m.c. arising in axial deformed nuclei within the prescription [6]. The average values are $\langle f \rangle_0 = \int d^3r f \rho_0 / A$ where ρ_0 is the g.s. density. As was checked, the c.m.c. remove spurious admixtures with very high accuracy.

The toroidal operator with the curl $\nabla \times \hat{\mathbf{j}}$ is vortical while the compression operator with the divergence $\nabla \cdot \hat{\mathbf{j}}$ is irrotational. Using the continuity equation, the current-dependent operator (2) can be transformed [6] to the familiar density-dependent form [25] $\hat{M}'_{\text{com}}(E1K) = 1/10 \int d^3r r \hat{\rho} [r^2 + d^s - 2d_K^a] Y_{1K}$ where $\hat{\rho}(\mathbf{r})$ is the density operator. This form is often used as a probe field in the analysis of (α, α') -reaction data for IS-GDR [25]. The calculated TDR and CDR strengths constituting IS-GDR in ^{24}Mg are shown in [37].

The QRPA calculations use a large two-quasiparticle (2qp) basis with the energies until ~ 100 MeV. For SLy6, the basis includes ≈ 1900 ($K=0$) and ≈ 3600 ($K=1$) states. For the photoabsorption, the Thomas-Reiche-Kuhn sum rule [55, 56] is exhausted by 100% (SLy6, SVbas) and 97% (SkM*). The isoscalar dipole energy-weighted sum rule [25] is exhausted by $\approx 97\%$.

In Fig. 2, the calculated toroidal ($\alpha = \text{tor}$) and compression ($\alpha = \text{com}$) values $B(E1K, \alpha)$ are shown for $I^\pi = 1^-$ QRPA states at the energy $5 < E < 10$ MeV (at $E < 5$ MeV our calculations do not give 1^- states). The transition operators (1) and (2) are used. Plot a) for SLy6 shows that the toroidal strength has an impressive $K=1$ peak at 7.92 MeV. What is important, this state is the *lowest* 1^- excitation. In the plot b), the irrotational compression strength is given by 7.92-MeV $K=1$ state and subsequent 9.56-MeV $K=0$ state (lowest among $K=0$ excitations). The exposure of the toroidal 7.92-MeV $K=1$ state in the compression response means that this state has a minor irrotational fraction. The middle and bottom plots of Fig. 2 show the responses calculated with SVbas and SkM*. The results noticeably deviate

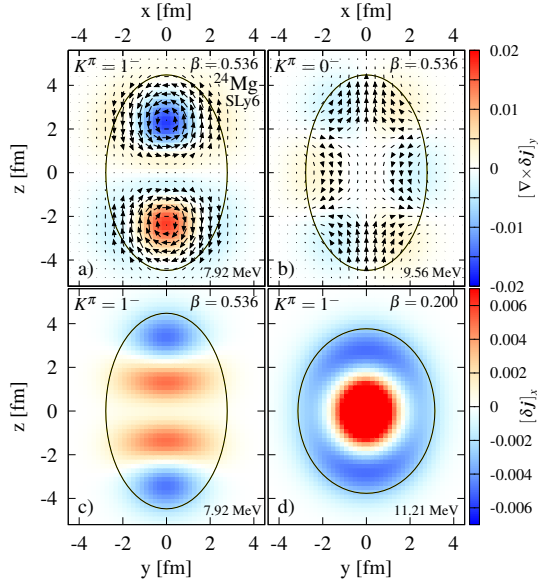


FIG. 3: (a-b): QRPA (SLy6) isoscalar dipole CTD $\delta \mathbf{j}_{zx}$ in z - x ($y=0$) plane for the states $K=1$ at $E=7.92$ MeV (left) and $K=0$ at $E=9.56$ MeV (right). Magnitude of $\delta \mathbf{j}_{zx}$ is determined by arrow lengths in arbitrary units. The vorticity $(\nabla \times \delta \mathbf{j})_y$ is shown by colors as indicated. (c-d) The CTD $\delta \mathbf{j}_x$ in z - y ($x=0$) plane for $K=1$ states computed at deformations $\beta=0.536$ (left, $E=7.92$ MeV) and $\beta=0.2$ (right, $E=11.21$ MeV). Unlike plots (a-b), the CTD are shown by colors. In all the plots, the nuclear surface is indicated by the solid line.

in details from SLy6 picture. However they also give the lowest toroidal $K=1$ state (at 7.26 MeV for SVbas and 8.19 MeV for SkM*) accompanied by the subsequent compression $K=0$ state. So the main result, individual toroidal $K=1$ state as the lowest 1^- excitation, is robust. The similar result was recently obtained within the Antisymmetrized Molecular Dynamics (AMD) approach in strongly deformed ^{10}Be [48].

The toroidal character of 7.92-MeV $K=1$ state is additionally justified in Fig. 3a) where its isoscalar current transition density (CTD) $\delta \mathbf{j}_{zx} = \langle \nu | (\hat{\mathbf{j}}_z + \hat{\mathbf{j}}_x) | 0 \rangle$ at the plane z - x ($y=0$) is shown. For simplicity, only convection part of the nuclear current is taken into account. Note that CTD by definition is fully determined by the structure of the QRPA ν -state and does not depend on the transition operators (1)-(2). Plot a) shows that the flow in $K=1$ state is indeed toroidal. Like in the schematic picture of Fig. 1d), its streamlines spin with opposite circulations around two parallel axes (perpendicular to z - x plane) in the top and bottom of the prolate system. At the same time, Fig. 3a) shows some important peculiarities. Unlike the toroidal pattern in spherical nuclei [7, 9, 13] and prolate ^{154}Sm [10] where the flow fills in most of the nuclear volume, here the flow is concentrated in the top and bottom of the nucleus and is almost absent in the equatorial region ($-0.8 \text{ fm} < z < 0.8 \text{ fm}$). So, in highly deformed ^{24}Mg , the torus-shaped vortex ring

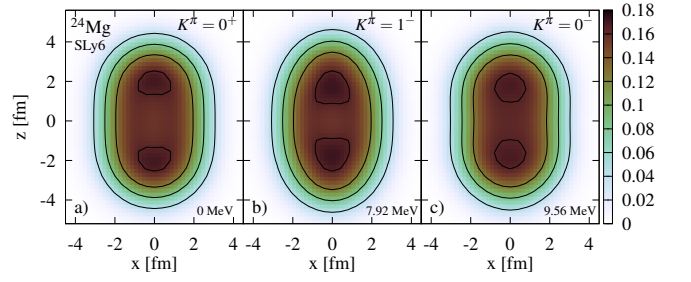


FIG. 4: QRPA (SLy6) densities (in fm^{-3}) of the ground state (a), 7.92-MeV $K=1$ state (b) and 9.56-MeV $K=0$ state (c).

converts into well separated vortex and antivortex. Both them are characterized by a high vorticity $(\nabla \times \delta \mathbf{j})_y$. Similar current fields take place for 7.26-MeV and 8.19-MeV $K=1$ states in SVbas and SkM* (not shown).

The character of the flow is even more clarified in the plot c) where CTD $\delta \mathbf{j}_x$ in z - y ($x=0$) plane embracing the vortex/antivortex axes is shown. We see that CTD indeed has opposite directions around $z \approx 3.5 \text{ fm}$ (blue) and 1.5 fm (red) in the top. The same is around -3.5 fm (blue) and -1.5 fm (red) in the bottom. The flows are maximal in these regions and vanish in the equatorial area, which corresponds to well separated vortex and antivortex. What is important, the flow in the plot c) does not form two elliptic areas (red surrounded by blue) like in the plot d) where CTD $\delta \mathbf{j}_x$ is shown for the toroidal 11.21-MeV $K=1$ state obtained at the small constrained deformation $\beta=0.2$. This proves that the current field in 7.92-MeV $K=1$ state of ^{24}Mg indeed acquires the vortex-antivortex configuration and that the high prolate deformation in ^{24}Mg is crucial for this transformation. By our knowledge, this result is the first demonstration of the transformation of the spherical Hill's vortex [14, 15] in a highly deformed confinement.

The toroidal 7.92-MeV $K=1$ state is mainly formed by two 2qp components, $pp[211 \uparrow -330 \uparrow]$ and $nn[211 \uparrow -330 \uparrow]$ (in Nilsson asymptotic quantum numbers), exhausting 54% and 39% of the norm, respectively. The comparison of Fig. 4a with the currents for these components (not shown) reveals that the toroidal flow is predominantly of 2qp origin. This agrees with the previous finding for ^{208}Pb [49].

For the comparison, in Fig. 3b) the CTD for $K=0$ state at 9.56 MeV is given. Its flow is basically irrotational. It is concentrated in four regions near the nuclear surface and vanishes at the nuclear center. The "static" intervals between these regions can be treated as compression ($z \sim -2 \text{ fm}$) and decompressions ($z \sim 2 \text{ fm}$) areas. This suggests that 9.56-MeV $K=0$ state is a compression mode.

The nucleus ^{24}Mg is known to demonstrate cluster properties [50–52]. Energies of 7.92-MeV $K=1$ and 9.56-MeV $K=0$ states are close to the α -particle threshold $S_\alpha = 9.3 \text{ MeV}$ [54] and so these states can be related to cluster degrees of freedom. A significant separation of

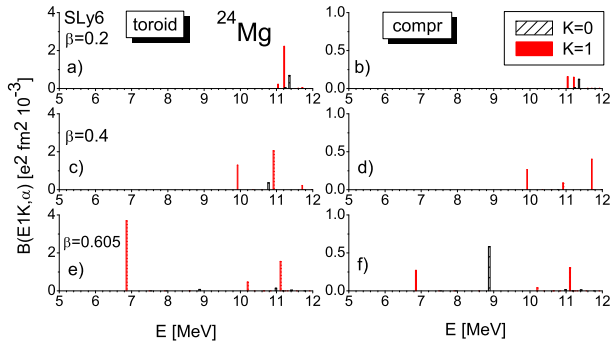


FIG. 5: Toroidal (left) and compression (right) $B(E1, \alpha)$ -values in ^{24}Mg , calculated with SLy6 for constrained deformations $\beta_2=0.2$ (upper), 0.4 (middle) and 0.605 (bottom). For each case, the $K=0$ (sparse black bars), and $K=1$ (filled red bars) states are depicted.

the vortex and antivortex in Fig. 3a) (in contrast to the toroidal flow covering all the nucleus interior in ^{154}Sm [10]) can also signal on the cluster structure. To check this, we show in Fig. 4 density distributions $\langle \nu | \hat{\rho} | \nu \rangle$ in z - x ($y=0$) plane for the ground state and QRPA states 7.92-MeV $K=1$ and 9.56-MeV $K=0$. In all these states, there are cumulations of density at the top and bottom of the nucleus, which can be interpreted as precursors of clustering, e.g. of α formation. The form of the cumulation regions and separation between them are somewhat different. Anyway we see that ^{24}Mg demonstrates a similar clustering in the ground state and dipole excitations around S_α . Perhaps this is a manifestation of mean-field/cluster duality pertinent to light nuclei [52]. The clustering can favor a significant spatial vortex/antivortex separation in the toroidal $K=1$ state and signify a possible α -vibrational contribution to the irrotational $K=0$ state. These aspects deserve a further investigation with more decisive observables [53].

A crucial role of the large axial prolate deformation is illustrated in Fig. 5. We see that, for the small deformation $\beta=0.2$, $K=1$ toroidal state lies at 11.2 MeV and is not the lowest one. At the larger deformation $\beta=0.4$, the toroidal strength is fragmented between two $K=1$ peaks where the lowest come down already to 9.9 MeV. Finally, at the experimental value $\beta=0.605$ [29], the toroidal $K=1$ strength is mainly concentrated in the lowest peak at 6.9 MeV, a feature which is well developed already at $\beta=0.536$ in Fig. 2a). Besides, at $\beta=0.605$, we get a concentration of the compression strength at 8.9 MeV. Altogether we see that the toroidal $K=1$ peak becomes the lowest and well separated state only at a high prolate deformation.

The toroidal 7.92-MeV $K=1$ state exhibits some collectivity. Its collective downshift (the difference between the QRPA energy and energy of the largest 2qp component) is 0.85 MeV, i.e. rather large. Besides, the state shows a strong $E3$ transition with $B(E3, 0^+0_{\text{g.s.}} \rightarrow$

$3^-1) = 402 \text{ e}^2\text{fm}^6$ (11.7 W.u.), which can be caused by the deformation-induced mixture of dipole and octupole modes and significant octupole correlations [58]. Though the state is mainly isoscalar, it also has a minor isovector fraction resulting in the isovector $E1$ decay to the ground state (g.s.) band: $B(E1, 1^-1 \rightarrow 0^+0_{\text{g.s.}}) = 2.52 \cdot 10^{-4} \text{ e}^2\text{fm}^2$. The experimental spectrum below 10 MeV in ^{24}Mg has three $I^\pi = 1^-$ states: at 7.555, 8.437 and 9.566 MeV [54]. Their K -assignment is rather ambiguous. Following Alaga rules [57], the toroidal 7.92-MeV $K=1$ state might correspond to 7.555-MeV or 8.437-MeV levels, see more details in [37].

In conclusion, our Skyrme QRPA calculations show that, in highly deformed axial ^{24}Mg , the *lowest* dipole $K=1$ state is a vortical toroidal excitation. Its computed energy (7.92 MeV for the Skyrme force SLy6) is close to the energies 7.555 and 8.437 MeV of two lowest 1^- levels in the experimental spectrum. This state is well separated from the surrounding spectrum and so represents the example of an *individual* toroidal state (TS). Following our analysis, TS becomes lowest due to the exceptionally high axial prolate deformation ($\beta_{\text{exp}}=0.605$) in ^{24}Mg . Perhaps, individual low-energy TS also exist in other strongly deformed light nuclei, e.g. in ^{10}Be [48], $^{20,22,24}\text{Ne}$ and $^{32,34}\text{Mg}$. $N=Z$ nuclei, like ^{24}Mg , are most promising since they do not have pygmy dipole admixtures.

The lowest energy of the $K=1$ TS in ^{24}Mg greatly simplifies its identification. TS should have peculiarities in (e, e') back scattering [19]. TS could serve as excellent test cases to probe various reactions for vortical nuclear excitations.

The toroidal nature of 7.92-MeV $K=1$ state is proved by a large toroidal strength and clear toroidal distribution of the nuclear current. Actually we get so-called Hill's vortex well known in hydrodynamics of turbulent fluids [14, 15]. Here we show for the first time, that, in a highly deformed axial confinement, Hill's vortex is transformed from toroidal to vortex-antivortex configuration.

The calculated nuclear density shows two clear well-separated cluster regions matching Hill's vortex and antivortex areas. The clustering takes place in the ground state and dipole toroidal $K=1$ and compressions $K=0$ states. Perhaps here we have an interesting interplay of clustering and vortical mean-field dynamics.

Main results persist for different Skyrme forces (SLy6, SV-bas, SkM*). Since the results are mainly caused by a huge axial prolate deformation, they can hardly be essentially changed by a possible triaxiality and coupling with complex configurations. Anyway we plan to scrutinize these effects in the subsequent studies.

V.O.N. thanks Profs. M.N. Harakeh and A. Diaz-Torres for valuable discussions. The work was partly supported by the Heisenberg - Landau (Germany - BLTP JINR), and Votruba - Blokhintsev (Czech Republic - BLTP JINR) grants. A.R. is grateful for support from

Slovak Research and Development Agency (Contract No. APVV-15-0225) and Slovak grant agency VEGA (Contract No. 2/0129/17). J.K. appreciates the support of the research plan MSM 0021620859 (Ministry of Education of the Czech Republic) and the Czech Science Foundation project P203-13-07117S.

-
- [1] V. M. Dubovik and A. A. Cheshkov, *Sov. J. Part. Nucl.* **5**, 318 (1975).
 - [2] S. F. Semenko, *Sov. J. Nucl. Phys.* **34**, 356 (1981).
 - [3] G. Colo, N. Van Giai, P.F. Bortignon, and M. R. Quaglia, *Phys. Lett. B* **485**, 362 (2000).
 - [4] D. Vretenar, N. Paar, P. Ring, and T. Nikšić, *Phys. Rev. C* **65**, 021301(R) (2002).
 - [5] N. Paar, D. Vretenar, E. Kyan, G. Colo, *Rep. Prog. Phys.* **70**, 691 (2007).
 - [6] J. Kvasil, V. O. Nesterenko, W. Kleinig, P.-G. Reinhard, and P. Vesely, *Phys. Rev. C* **84**, 034303 (2011).
 - [7] A. Repko, P.-G. Reinhard, V. O. Nesterenko, and J. Kvasil, *Phys. Rev. C* **87**, 024305 (2013).
 - [8] P.-G. Reinhard, V. O. Nesterenko, A. Repko, and J. Kvasil, *Phys. Rev. C* **89**, 024321 (2014).
 - [9] V. O. Nesterenko, J. Kvasil, A. Repko, W. Kleinig, P.-G. Reinhard, *Phys. Atom. Nucl.* **79**, 842 (2016).
 - [10] A. Repko, J. Kvasil, V. O. Nesterenko, and P.-G. Reinhard, *Eur. Phys. J. A* **53**, 221 (2017).
 - [11] S. I. Bastrukov, S. Mişicu, and A. V. Sushkov, *Nucl. Phys. A* **562**, 191 (1993).
 - [12] S. Mişicu, *Phys. Rev. C* **73**, 024301 (2006).
 - [13] N. Ryezayeva, T. Hartmann, Y. Kalmykov, H. Lenske, P. von Neumann-Cosel, V. Yu. Ponomarev, A. Richter, A. Shevchenko, S. Volz, and J. Wambach, *Phys. Rev. Lett.* **89**, 272502 (2002).
 - [14] M. J. M. Hill, *Phil. Trans. Roy. Soc. London A* **185**, 213 (1894).
 - [15] L. M. Mame-Thomson, *Theoretical hydrodynamics*, 4th ed., ch. 18 (Macmillan, New York, 1960).
 - [16] D. Vretenar, A. Wandelt, and P. Ring, *Phys. Lett. B* **487**, 334 (2000).
 - [17] M. N. Harakeh, K. van der Borg, T. Ishimatsu, H. P. Morsch, A. van der Woude, and F. E. Bertrand, *Phys. Rev. Lett.* **38**, 676 (1977).
 - [18] S. Stringari, *Phys. Lett. B* **108**, 232 (1982).
 - [19] A. Richter, *Nucl. Phys. A* **731**, 59 (2004).
 - [20] E. Bravo and G. Martínez-Pinedo, *Phys. Rev. C* **85**, 055805 (2012).
 - [21] V.M. Dubovik and V.V. Tugushev, *Phys. Rep.* **187**, 145 (1990).
 - [22] I. Fernandez-Corbaton, S. Nanz, and C. Rockstuhl, *Scien. Reports* **7**, 7527 (2016).
 - [23] S.I. Bastrukov, D.V. Podgany, J. Yang, and F. Weber, *JETP* **95**, 789 (2002).
 - [24] Chiu Man Ho and R.J. Scherrer, *Phys. Lett. B* **722**, 341 (2013).
 - [25] M. N. Harakeh and A. van der Woude, *Giant Resonances* (Clarendon Press, Oxford, 2001).
 - [26] D. H. Youngblood, Y.-W. Lui, H. L. Clark, B. John, Y. Tokimoto, X. Chen, *Phys. Rev. C* **69**, 034315 (2004).
 - [27] D. H. Youngblood, Y.-W. Lui, B. John, Y. Tokimoto, H. L. Clark, and X. Chen, *Phys. Rev. C* **69**, 054312 (2004).
 - [28] M. Uchida, H. Sakaguchi, M. Itoh, M. Yosoi, T. Kawabata, Y. Yasuda, H. Takeda, T. Murakami, S. Terashima, S. Kishi, U. Garg, P. Boutachkov, M. Hedden, B. Khararaja, M. Koss, B. K. Nayak, S. Zhu, M. Fujiwara, H. Fujimura, H. P. Yoshida, K. Hara, H. Akimune, and M. N. Harakeh, *Phys. Rev. C* **69**, 051301(R) (2004).
 - [29] S. Raman, C. W. Nestor, Jr., and P. Tikkanen, *At. Data and Nucl. Data Tables* **78**, 1 (2001).
 - [30] M. Bender, P.-H. Heenen, and P.-G. Reinhard, *Rev. Mod. Phys.* **75**, 121 (2003).
 - [31] A. Repko, J. Kvasil, V. O. Nesterenko, and P.-G. Reinhard, arXiv:1510.01248[nucl-th].
 - [32] E. Chabanat, P. Bonche, P. Haensel, J. Meyer, and R. Schaeffer, *Nucl. Phys. A* **635**, 231 (1998).
 - [33] P. Klupfel, P.-G. Reinhard, T. J. Burvenich, and J. A. Maruhn, *Phys. Rev. C* **79**, 034310 (2009).
 - [34] J. Bartel, P. Quentin, M. Brack, C. Guet, and H.-B. Haakansson, *Nucl. Phys. A* **386**, 79 (1982).
 - [35] W. Kleinig, V. O. Nesterenko, J. Kvasil, P.-G. Reinhard and P. Vesely, *Phys. Rev. C* **78**, 044313 (2008).
 - [36] J. Kvasil, A. Repko, V. O. Nesterenko, W. Kleinig, and P.-G. Reinhard, *Int. J. Mod. Phys. E*, **21**, 1250041 (2012).
 - [37] See Supplemental Material [url] with additional Refs. [38-42].
 - [38] B.S. Ischkanov, I.M. Kapitonov, E.I. Lileeva, E.V. Shirokov, V.A. Erokhova, M.A. Elkin, A.V. Izotova, Report MSU-INP-2002-27/711 (2002).
 - [39] V.V. Varlamov, M.E. Stepanov, V.V. Chesnokov, *J. Bull. Russ. Acad. Sci.* **67**, 724 (2003).
 - [40] J. Kvasil, V. O. Nesterenko, W. Kleinig, and P. - G. Reinhard, *Phys. Scr.* **89**, 054023 (2014).
 - [41] D. Branford, N. Gardner, and I.F. Wright, *Phys. Lett. B*, **36**, 456 (1971).
 - [42] L.K. Fiefield, E.F. Garman, M.J. Hurst, T.J.M. Symons, F. Watt, C.H. Zimmerman, and K.W. Allen, *Nucl. Phys. A* **322**, 1 (1979).
 - [43] T.R. Rodriguez and J.L. Egido, *Phys. Rev. C* **81**, 064323 (2010).
 - [44] M. Bender and P.-H. Heenen, *Phys. Rev. C* **78**, 024309 (2008).
 - [45] J. M. Yao, H. Mei, H. Chen, J. Meng, P. Ring, and D. Vretenar, *Phys. Rev. C* **83**, 014308 (2011).
 - [46] N. Hinohara and Y. Kanada-En'yo, *Phys. Rev. C* **83**, 014321 (2011).
 - [47] M. Kimura, R. Yoshida, and M. Isaka, *Prog. Theor. Phys.*, **127**, 287 (2012).
 - [48] Y. Kanada-Enyo and Y. Shikata, *Phys. Rev. C* **95**, 064319 (2017).
 - [49] V.O. Nesterenko, A. Repko, P.-G. Reinhard, and J. Kvasil, *EPJ Web of Conferences*, **93**, 01020 (2015).
 - [50] P.A. Butler and W. Nazarevitz, *Rev. Mod. Phys.*, **68**, 349 (1996).
 - [51] W.N. Catford, *The Nucleus: New Physics for the New Millennium*, ed. F.D. Smit, R. Lindsay and S.V. Fortsch (Kluwer Academic Press/Plenum Publishers, NY, 2000), p. 127.
 - [52] Y. Chiba and M. Kimura, *Phys. Rev. C* **91**, 061302(R) (2015).
 - [53] P.-G. Reinhard, J. A. Maruhn, A. S. Umar, and V. E. Oberacker, *Phys. Rev. C* **83**, 034312 (2011).
 - [54] Database [http://www.nndc.bnl.gov].
 - [55] P. Ring and P. Schuck, *The Nuclear Many-Body Problem* (Springer-Verlag, Berlin, 1980).

- [56] V. O. Nesterenko, W. Kleinig, J. Kvasil, P. Vesely, and P.-G. Reinhard, *Int. J. Mod. Phys. E* **17**, 89 (2008).
- [57] G. Alaga, *Phys. Rev.* **100**, 432 (1955).
- [58] H. Noto, *Prog. Theor. Phys.*, **66**, 195 (1981).